Supporting Information for "Isopycnal eddy stirring dominates thermohaline mixing in the upper subpolar North Atlantic"

Bieito Fernández Castro[1], Daniel Fernández Román[2], Bruno Ferron[3], Marcos Fontela[4], Pascale Lherminier[3], Alberto Naveira Garabato[1], Fiz F. Pérez[4], Carl Spingys[5], Kurt Polzin[6], and Antón Velo[4]

[1]Ocean and Earth Science, National Oceanography Centre, University of Southampton, Southampton, UK

[2]Centro de Investigacións Mariñas, Universidade de Vigo (CIM-UVigo), Vigo, Spain

[3]Univ Brest, CNRS, Ifremer, IRD, Laboratoire d'Océanographie Physique et Spatiale (LOPS), IUEM, F29280, Plouzané, France

[4]Instituto de Investigacións Mariñas, IIM-CSIC, Vigo, Spain

[5]National Oceanography Centre, Southampton, UK

[6]Woods Hole Oceanographic Institution, Woods Hole, USA

Contents of this file

Supplementary text: Uncertainty assessment

Our triple decomposition approach involves filtering density-compensated thermohaline fine structures from the measured property profiles to obtain "mean flow" profiles (θ^{m}, S^{m}) and to diagnose the rate of downscale variance transfer by small-scale turbulence ($P^{\perp}$). We chose to compute θ^{m} and S^{m} through a polynomial fit of the observed $\overline{\theta}$ and $\overline{S}$ with respect to σ_θ. This choice involves an element of subjectivity and uncertainty. Furthermore, by construction of the approach, any misfit between the polynomial fit and the actual $\overline{\theta}$ and $\overline{S}$ tends to be density-compensated, resulting in a potential overestimation of the effect of isopycnal stirring.

To gauge how this uncertainty may affect our conclusions, we tested an alternative method using time-series station dataset, where we have enough data to estimate mean flow profiles by performing a temporal average. To obtain θ^{m} and S^{m} for each vertical cast, we first calculated time-mean $\overline{\theta}$ and $\overline{S}$ profiles as a function of σ_θ and then interpolated them onto the observed σ_θ from each cast. The vertical distribution and overall magnitude of the alternative $P^{\perp}$ profiles generally agree with the original results, although depth-averaged P_{θ^2} and $P^{\perp}_{S^2}$ are roughly 30% and 70% lower, respectively (Fig. S3). This implies a larger contribution of isopycnal stirring than originally estimated. Thus, the potential overestimation of isopycnal stirring resulting from model misfit does not appear to be relevant here. Instead, the apparent underestimation may arise from fitting a 4-degree polynomial to more slowly varying $\overline{\theta}, \overline{S}$, which may produce spurious vertical gradients on the scale of $\sim$100 m and below, not relevant for the real distribution of θ^m, S^m across

isopycnals. At any rate, while there is some uncertainty associated with our calculations, the prevalence of isopycnal over diapycnal mixing emerges as a highly robust result.

The salinity budget is also subject to uncertainties stemming from the use of the Osborn and Cox (1972) formula (Eq. 8) to estimate χ_S, assuming a local balance between dissipation (χ_S) and production by small-scale turbulence acting on fine-scale gradients (P_{S^2}). The accuracy of this approximation is supported by the good agreement between the corresponding terms in the temperature variance equation (Fig. 2). To bolster our confidence further, we repeated the temperature variance analysis presented in Fig. 4 using P_{θ^2} instead of χ_θ and found excellent agreement with the original computations (Fig. S4).

There are two other potential sources of uncertainty and bias in the triple decomposition approach: the assumptions of a constant mixing efficiency ($\Gamma = 0.2$), and a negligible contribution of double diffusive processes to variance dissipation. The former assumption is again strongly supported by the good agreement between χ_θ and $P^{\perp}_{\theta^2}$ (Fig. 2), and consistent with the dominant regime of turbulence in the region, with ∼70% of our data below 50 m laying on intermediate values of the buoyancy Reynolds number ($Re_b = 10 - 500$, Fig. S5). In this Re_b range, mixing efficiency is expected to be relatively constant at ∼0.2 (Ijichi et al., 2020).

The importance of double diffusion can also be ruled out on similar grounds, as turbulence in the intermediate regime is likely to hamper the development of double diffusive instabilities (St Laurent & Schmitt, 1999). Further, stratification conditions potentially conducive to double diffusive instabilities are only observed in the WEB, due to unstable salinity stratification (Fig. 1c). However, the density ratio, $R_\rho = (\alpha\,\partial\overline{\theta}/\partial z)/(\beta\,\partial\overline{S}/\partial z)$,

is systematically greater than 2 (not shown), indicating only weak salt fingering instability, which would be easily disrupted by shear-driven turbulence (St Laurent & Schmitt, 1999). This is consistent with the lack of thermohaline fine-scale staircase structures, characteristic of double diffusion, throughout the BOCATS2 section.

References

Ijichi, T., St. Laurent, L., Polzin, K. L., & Toole, J. M. (2020). How Variable Is Mixing Efficiency in the Abyss? *Geophysical Research Letters*, *47*(7), e2019GL086813. doi: 10.1029/2019GL086813

Osborn, T. R., & Cox, C. S. (1972, January). Oceanic fine structure. *Geophysical Fluid Dynamics*, *3*(1), 321–345. doi: 10.1080/03091927208236085

St Laurent, o., & Schmitt, R. W. (1999). The Contribution of Salt Fingers to Vertical Mixing in the North Atlantic Tracer Release Experiment. *Journal of Physical Oceanography*, *29*(7), 1404–1424. doi: 10.1175/1520-0485(1999)029⟨1404:TCOSFT⟩2.0.CO;2

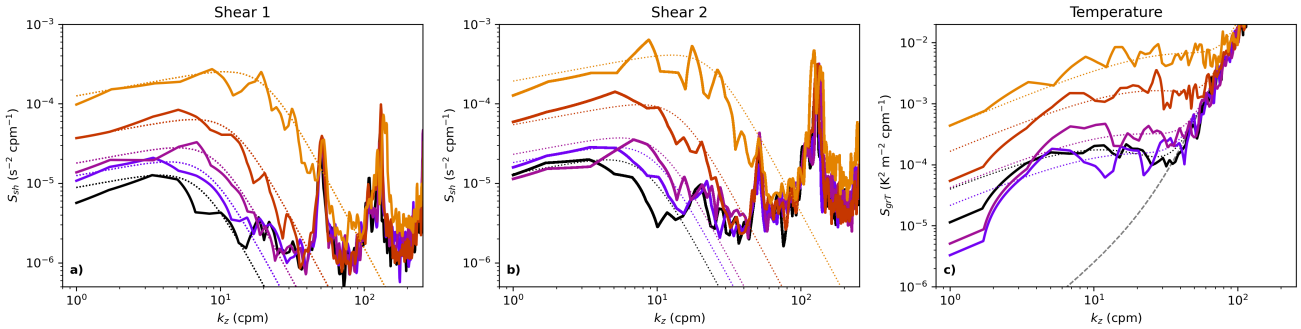

Figure S1. Randomly selected shear and temperature gradient wavenumber (k_z) spectra, from shear sensor 1 (a), shear sensor 2 (b), and thermistor (c), respectively, and for ε values in the range $10^{-10} - 10^{-6}$ W/kg (spectra are shown in black for low ε, and move from blue to orange for for higher ε). Dotted lines show the corresponding empirical spectra obtained through spectral integration (shear) or fitting to the Kraichnan spectrum (temperature). The thermistor theoretical noise curve is shown as a gray dashed line.

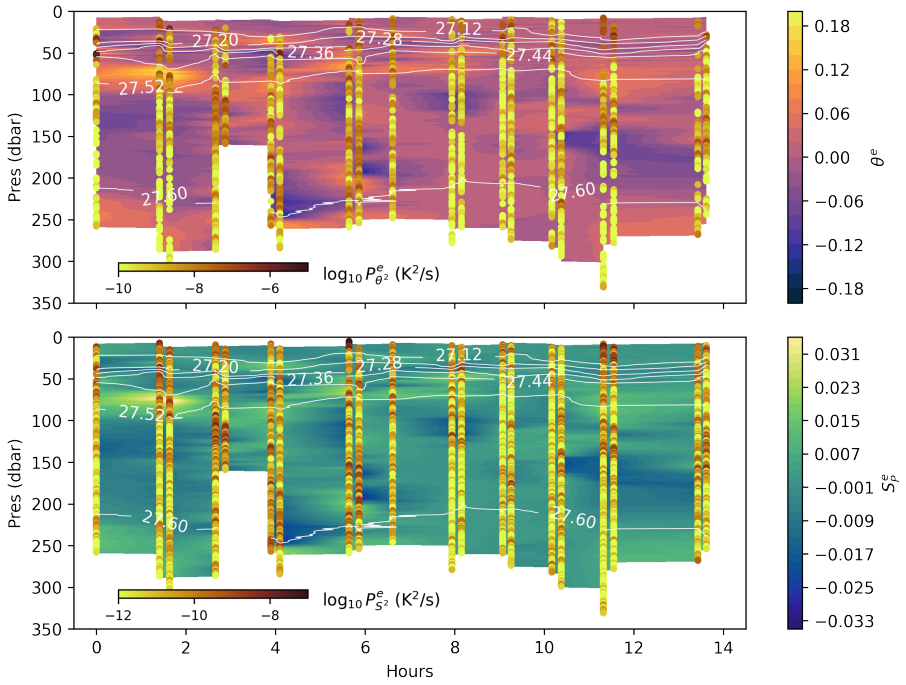

Figure S2. a) potential temperature (θ^e) and salinity (S^e) mesoscale anomaly profiles for the time-series observation in station 32 over the Reykjanes Ridge. Potential density contours (white) are overlaid, and small-scale temperature ($P^e_{\theta^2}$) and salinity ($P^e_{S^2}$) variance production by isopcynal eddy stirring are shown as colored dots.

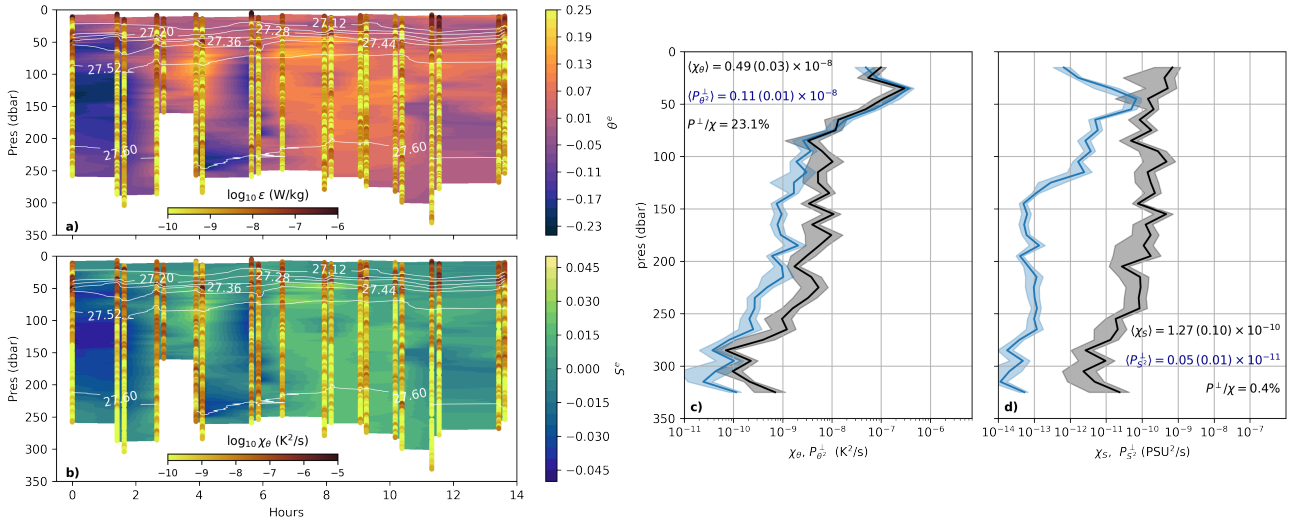

Figure S3. Same as Fig. 3 but with an alternative computation of $P^{\perp}_{\theta^2}$ and $P^{\perp}_{S^2}$ based on the time-mean profiles of $\overline{\theta}$ and $\overline{S}$ as a function of σ_θ. Panels a) and b) show potential temperature and salinity mesoscale anomaly profiles (θ^e, S^e, respectively) computed using the alternative method (Supplementary Text 1).

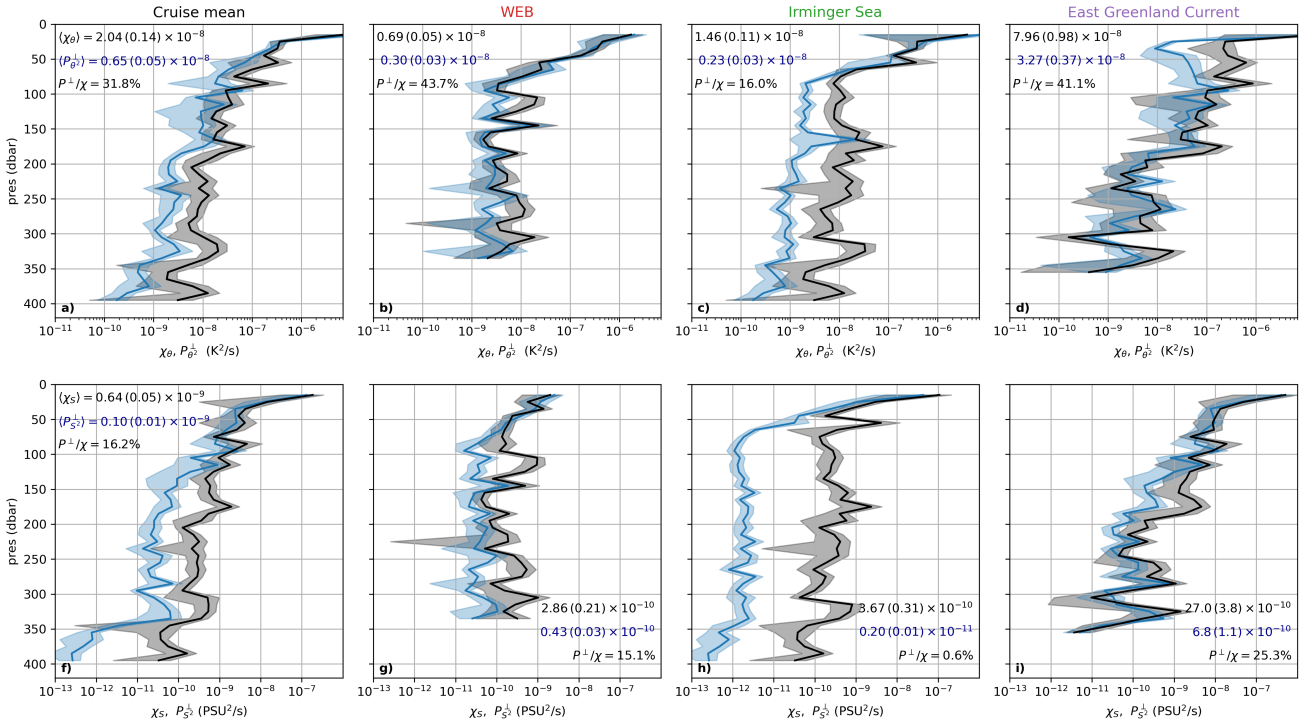

Figure S4. Same as Fig. 4 but with χ_θ estimated using the Osborn and Cox (1972) formula (Eq. 2) instead of the measured χ_θ.

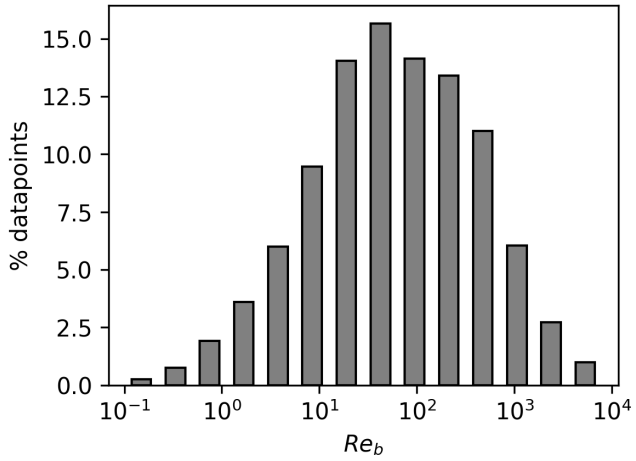

Figure S5. Histogram of the buoyancy Reynolds number ($Re_b = \varepsilon/(\nu N^2)$, where ν is molecular viscosity). Includes all of the cruise data below 50 m depth.